SUPPLEMENTAL MATERIAL

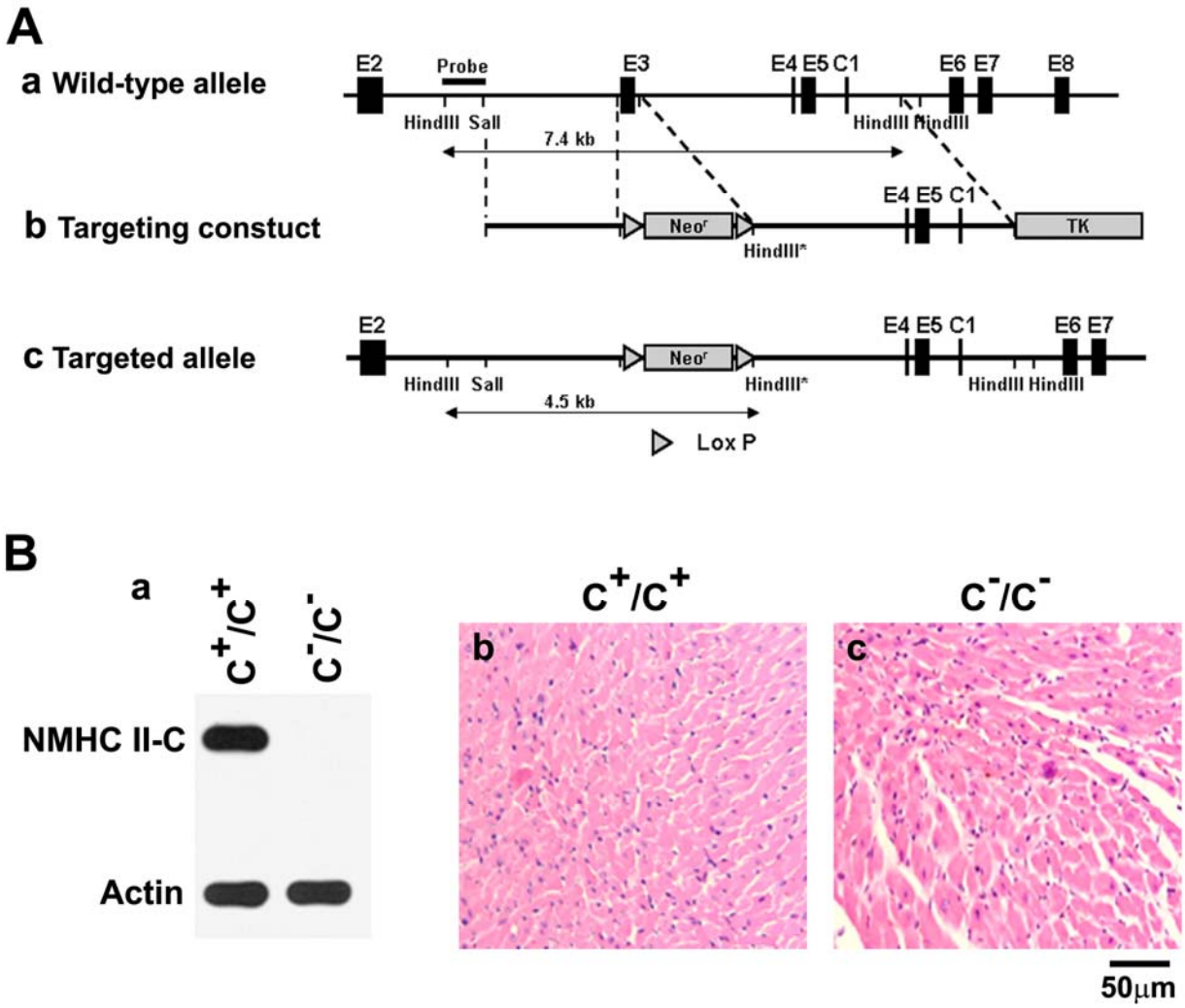

Fig. S1. Schematic Diagram and Characterization of NMHC II-C Ablated Mice. (Aa) Wild-type NMHC II-C allele, (b) targeting construct for NMHC II-C ablation and (c) targeted NMHC II-C null allele. Black rectangles, exons; thin black line, intron; gray rectangles, selection cassettes. Probe used for genotyping is indicated. The Neo^r cassette includes a HindIII site denoted by HindIII*. (Ba) Immunoblot demonstrating absence of NMHC II-C in lungs of C^-/C^- mouse. (b,c) H&E staining of heart sections from 5-month C^+/C^+ (b) and C^-/C^- (c) mice. No obvious pathological defects are seen in C^-/C^- hearts compared to C^+/C^+ hearts.

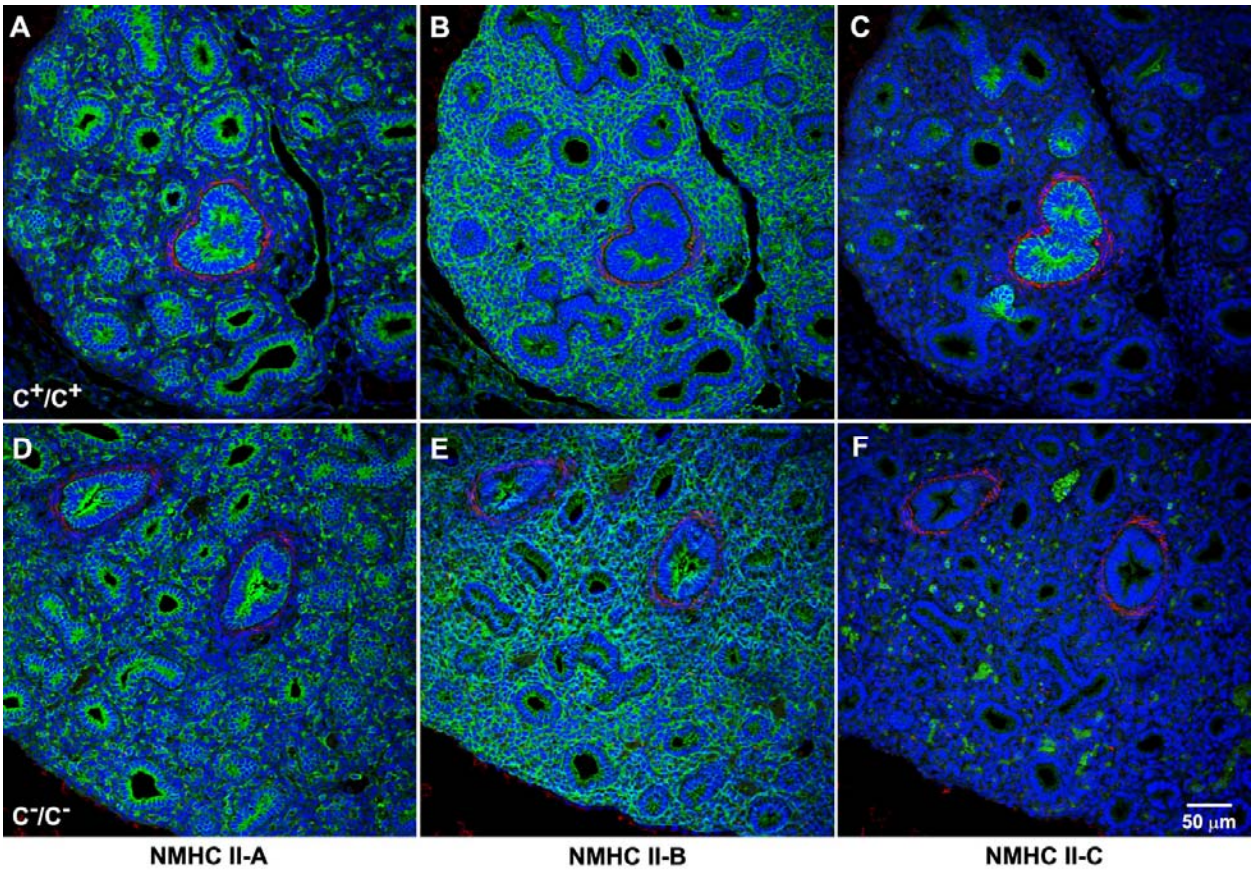

Fig. S2. NM II-C Null Mice Develop Normal Lungs with No Changes in NM II-A and II-B Expression. Immunofluorescence confocal images of serial sections from E13.5 wild-type (A-C) and C^-/C^- (D-F) mouse lungs stained for NMHC II-A (green, A,D), II-B (green, B,E), and II-C (green, C,F) together with desmin (red, a marker for smooth muscle cells). There is no change in the expression of NM II-A and II-B between wild-type (A,B) and C^-/C^- (D,E) lungs. NM II-C is only expressed in the epithelial cells of wild-type lungs (C) and is not detected in C^-/C^- lung (F). The green fluorescence spots seen in F are due to red blood cells. DAPI (blue) stains the nuclei.

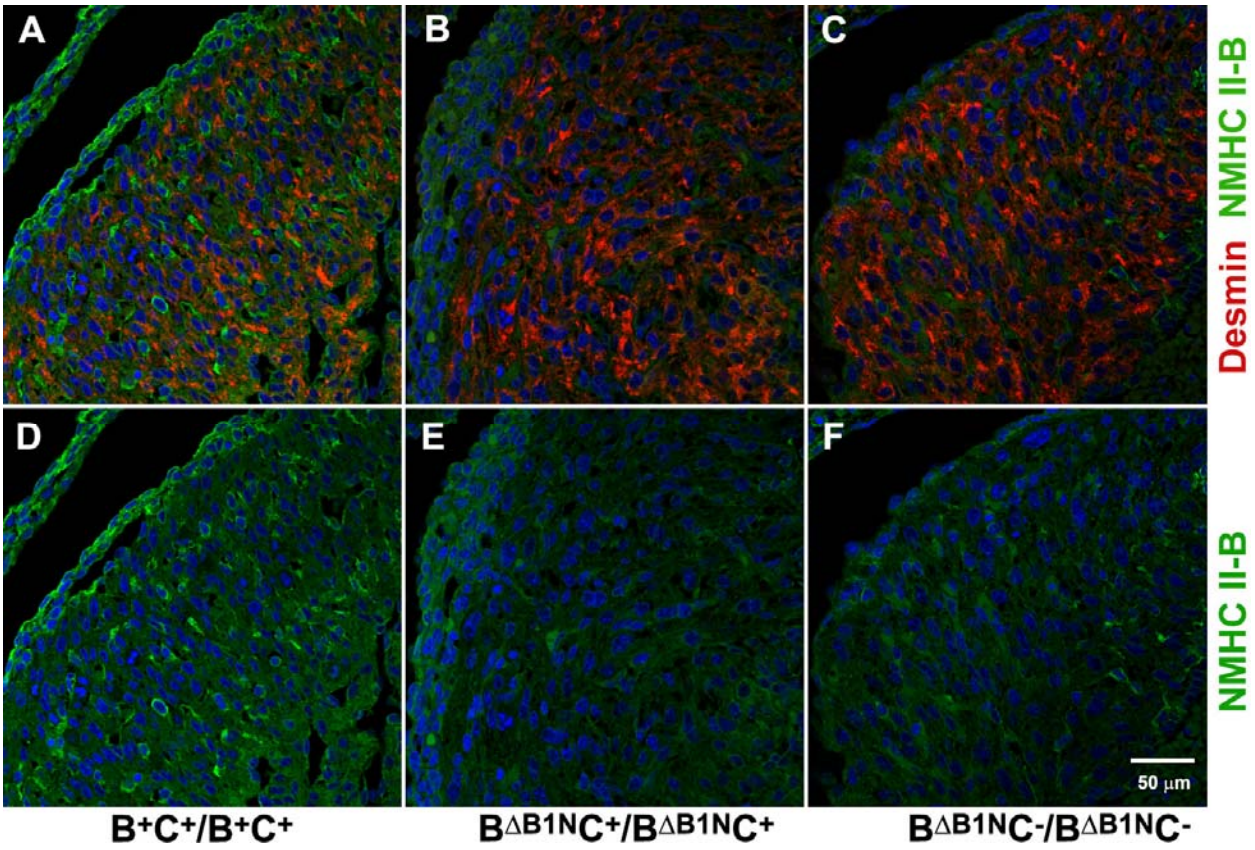

Fig. S3. Ablation of NM II-C Does Not Affect NM II-B Expression in $B^{\Delta B1N}C^{-}/B^{\Delta B1N}C^{-}$ Mouse Hearts. Immunofluorescence confocal images of heart sections from E13.5 $B^{+}C^{+}/B^{+}C^{+}$ (A,D) $B^{\Delta B1N}C^{+}/B^{\Delta B1N}C^{+}$ (B,E), and $B^{\Delta B1N}C^{-}/B^{\Delta B1N}C^{-}$ (C,F) mice stained for NMHC II-B (green, A,D), and desmin (red, a marker for cardiac myocytes, A-C). Both $B^{\Delta B1N}C^{+}/B^{\Delta B1N}C^{+}$, $B^{\Delta B1N}C^{-}/B^{\Delta B1N}C^{-}$ hearts show marked decrease in NM II-B expression compared to wild-type hearts. No obvious difference is seen in the level of NM II-B expression between $B^{\Delta B1N}C^{+}/B^{\Delta B1N}C^{+}$ and $B^{\Delta B1N}C^{-}/B^{\Delta B1N}C^{-}$ hearts. DAPI (blue) stains the nuclei.

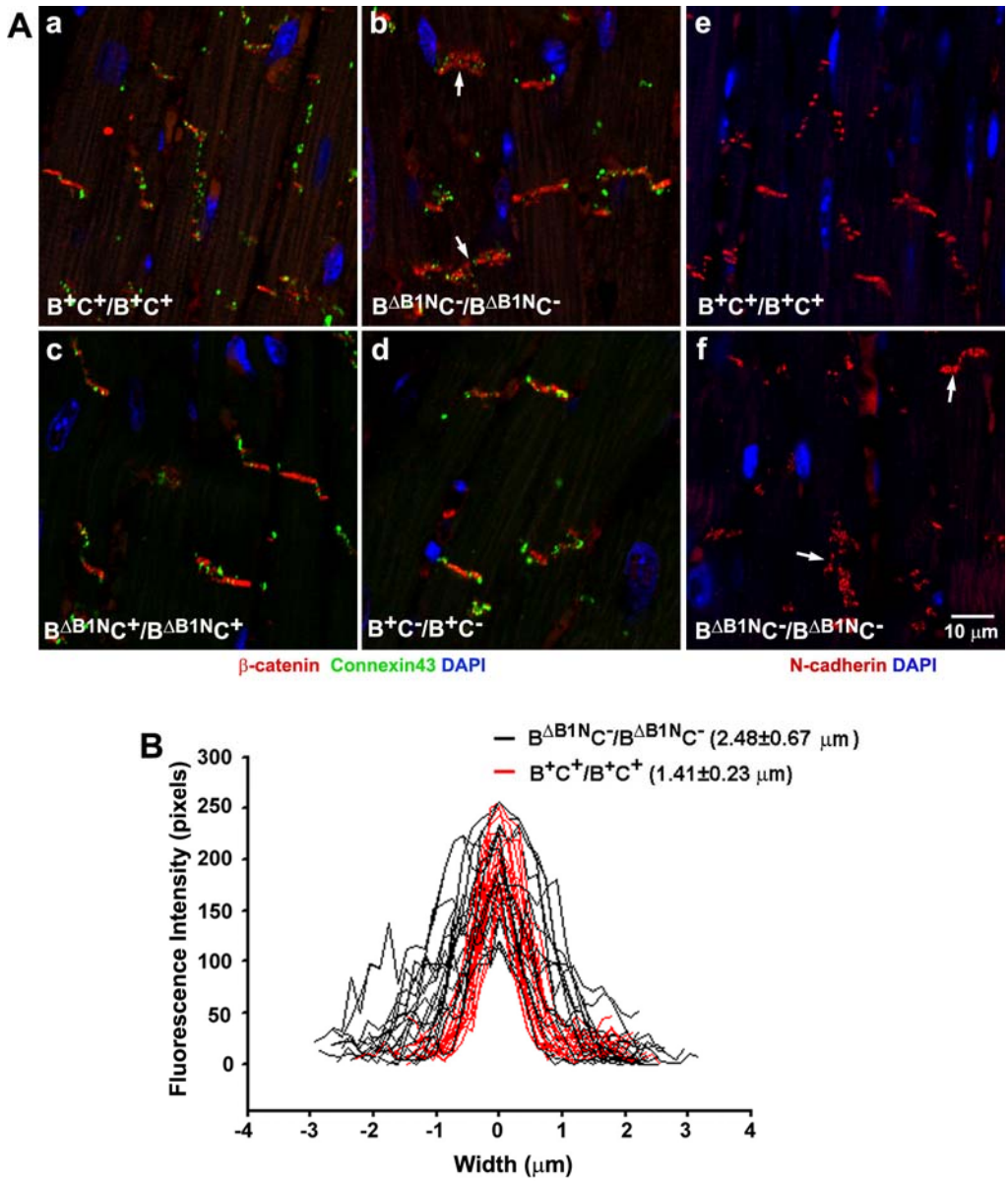

Fig. S4. Impaired Localization of β-Catenin and N-cadherin in $B^{\Delta B1N}C^{-}/B^{\Delta B1N}C^{-}$ Intercalated Discs. (A) Immunofluorescence confocal images of adult heart sections from $B^{+}C^{+}/B^{+}C^{+}$, $B^{\Delta B1N}C^{-}/B^{\Delta B1N}C^{-}$, $B^{\Delta B1N}C^{+}/B^{\Delta B1N}C^{+}$, and $B^{+}C^{-}/B^{+}C^{-}$ mice stained for β-catenin (red, a-d), connexin43 (green, a-d) and N-cadherin (red, e,f). In contrast to $B^{+}C^{+}/B^{+}C^{+}$(a,e), $B^{+}C^{-}/B^{+}C^{-}$ (d), and $B^{\Delta B1N}C^{+}/B^{\Delta B1N}C^{+}$ (c) cardiac myocytes where β-catenin and N-cadherin very precisely stain the intercalated discs, $B^{\Delta B1N}C^{-}/B^{\Delta B1N}C^{-}$ myocytes (arrows, b,f) show a diffuse β-catenin and N-cadherin staining. No difference in connexin43 staining (green, a-d) is observed among these four genotypes. Nuclei were stained by DAPI (blue). (B) Profiles of β-catenin staining at the intercalated discs for $B^{+}C^{+}/B^{+}C^{+}$ (red lines) and $B^{\Delta B1N}C^{-}/B^{\Delta B1N}C^{-}$ (black lines) mouse hearts. $B^{\Delta B1N}C^{-}/B^{\Delta B1N}C^{-}$ hearts showed a diffuse β-catenin distribution manifested by widened β-catenin staining at the intercalated discs compared to the wild-type hearts. An embedded Zeiss LSM image profile tool is used to quantify the fluorescence intensity along a line drawn vertically across the intercalated discs.

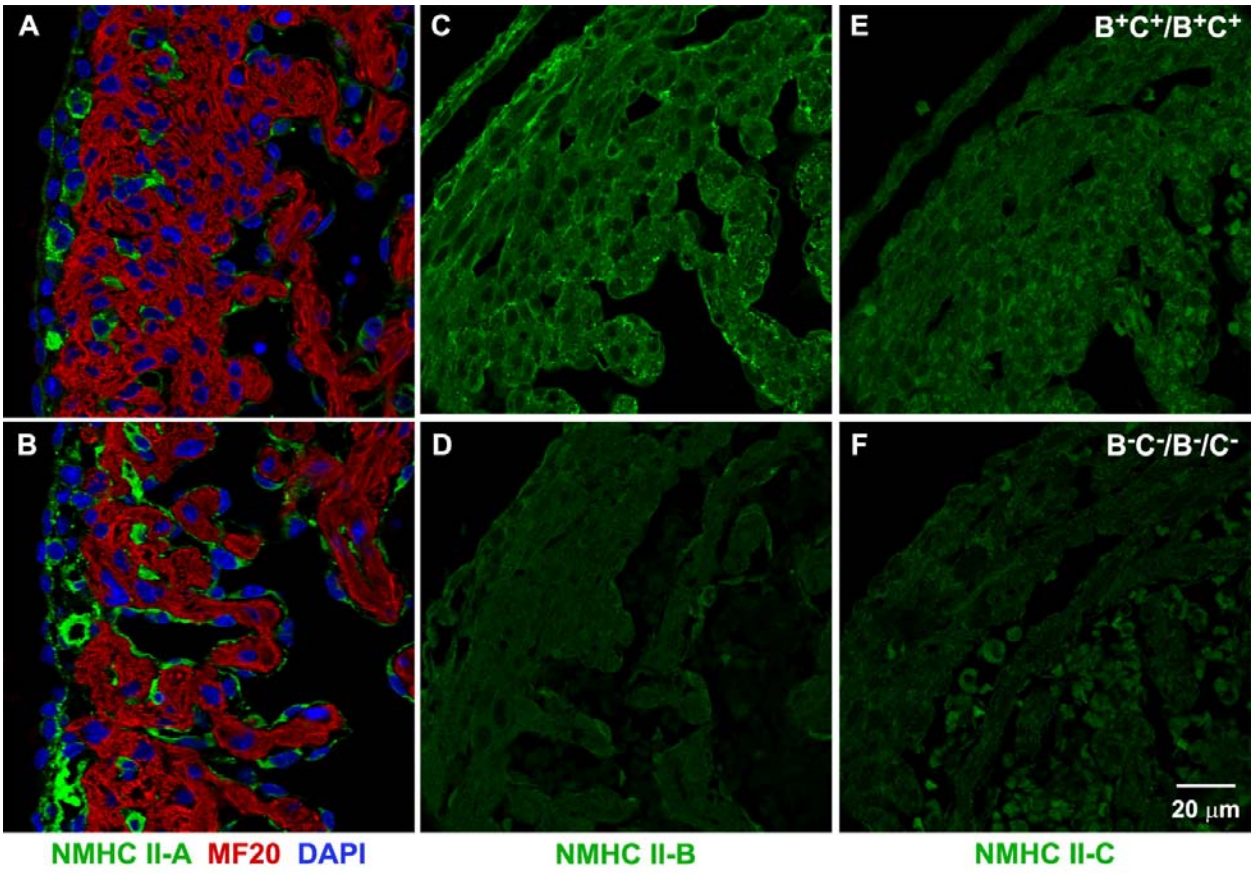

Fig. S5. Simultaneous Ablation of NM II-B and II-C in B^-C^-/B^-C^- Hearts. Immunofluorescence confocal images of heart sections from E13.5 B^+C^+/B^+C^+ (A, C, and E) and B^-C^-/B^-C^- (B, D, and F) mice stained with antibodies to NMHC II-A (green, A,B), II-B (green, C,D) and II-C (green, E,F), and MF20 (red, a marker for cardiac myocytes, A,B). Panels A and B are merged images of NMHC II-A (green), MF20 (red) and DAPI (blue, nuclei) staining. In both B^+C^+/B^+C^+ (A) and B^-C^-/B^-C^- (B) hearts NMHC II-A only stains the non-myocytes. B^+C^+/B^+C^+ hearts showed diffuse staining of NMHC II-B (C) and II-C (E) at this age. Neither NMHC II-B (D) nor II-C (F) is detected in B^-C^-/B^-C^- hearts.

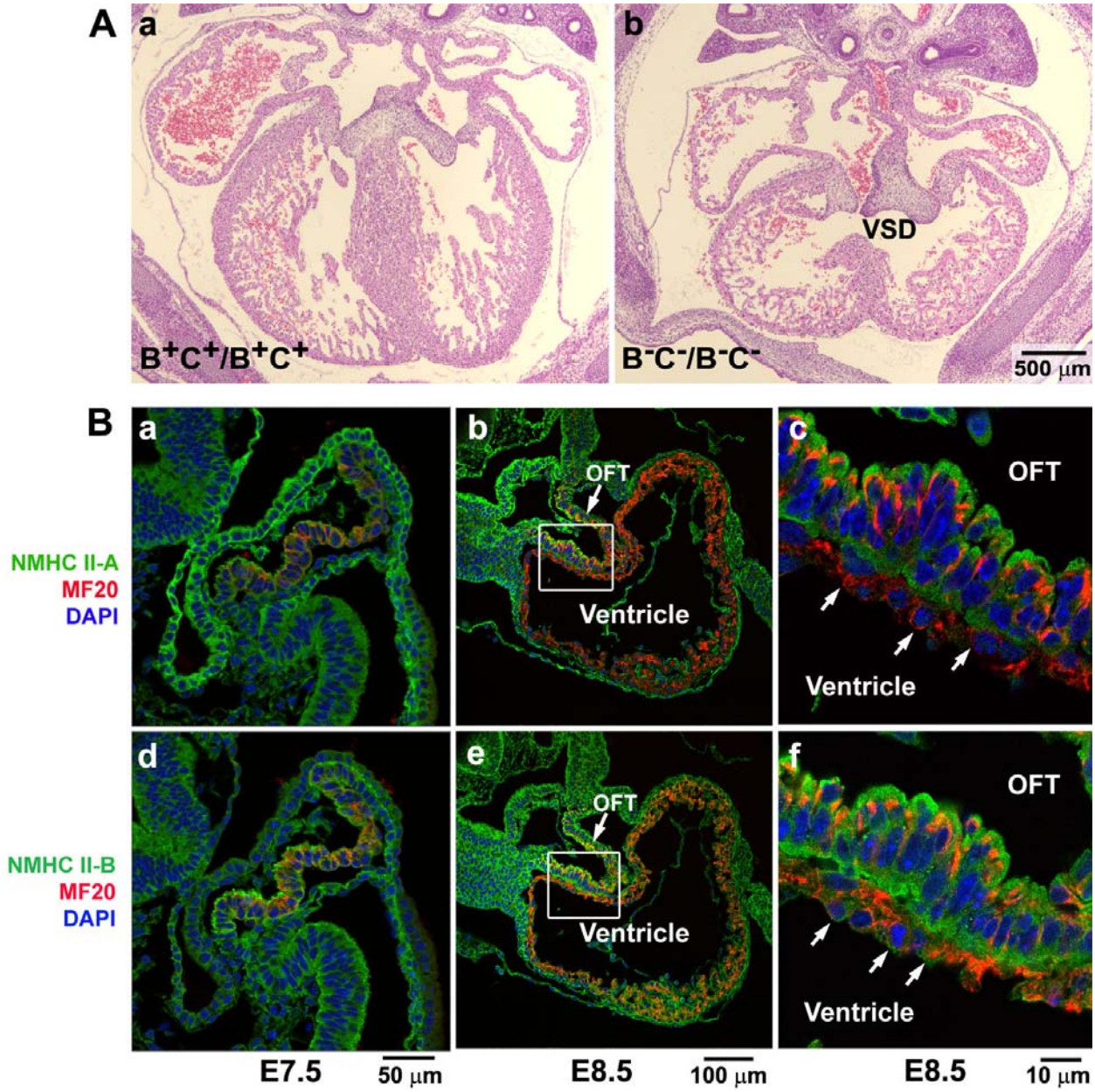

Fig. S6. Expression of NM II during Early Heart Formation. (A) H&E stained mouse heart sections from B^+C^+/B^+C^+ (a) and B^-C^-/B^-C^- (b) mice at E13.5. The B^-C^-/B^-C^- heart is hypoplastic with a very thin compact myocardium and ventricular septal defect (VSD, b), but develops four chambers. (B) Immunofluorescence confocal images of wild-type mouse hearts at E7.5 and E8.5 stained for NMHC II-A (green, a-c) and II-B (green, d-f), and co-stained for MF20 (red, a marker for cardiac myocytes). At E7.5, the early cardiac myocytes (a,d) show co-staining of NMHC II-A and MF20 (a) or NMHC II-B and MF20 (d) indicating that both NMHC II-A and II-B are expressed in cardiac myocytes at this stage. At E8.5, the cardiac myocytes in the developing outflow tract (OFT) still express both NMHC II-A (b, magnified in c) and II-B (e, magnified in f), however in the ventricular myocytes at E8.5 (arrows, c,f) only NMHC II-B (e,f), and not NMHC II-A (b,c) is detected.

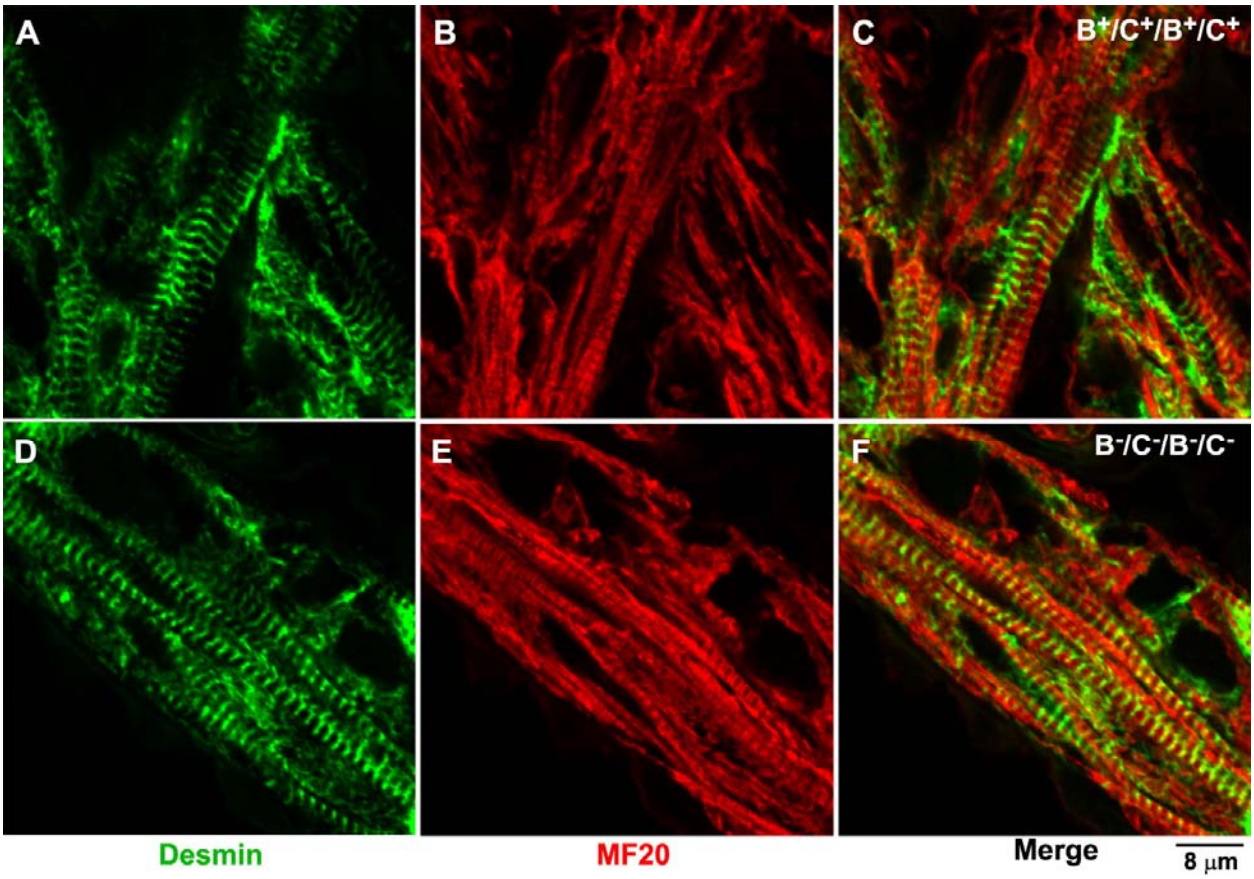

Fig. S7. Normal Sarcomere Formation in B^-C^-/B^-C^- Cardiac Myocytes.
Immunofluorescence confocal images of E13.5 cardiac myocytes stained with MF20 (red, a marker for cardiac myosin II, B,E) and desmin (green, A,D) in B^+C^+/B^+C^+ (A-C) and B^-C^-/B^-C^- (D-F) mouse hearts. No difference in sarcomere formation is found between B^+C^+/B^+C^+ and B^-C^-/B^-C^- hearts.